International Journal of Nanomedicine

Dovepress
open access to scientific and medical research

Open Access Full Text Article

ORIGINAL RESEARCH

A New Type of $MgFe_2O_4$@CuS-APTES Nanocarrier for Magnetic Targeting and Light-Microwave Dual Controlled Drug Release

This article was published in the following Dove Press journal:
International Journal of Nanomedicine

Hongxia Peng[1,2]
Menglin Wang[1]
Chuanyue Hu[1]
Jun Guo[1]

[1]Hunan Provincial Key Laboratory of Fine Ceramics and Powder Materials, Hunan University of Humanities, Science and Technology, Lou'di, Hunan, People's Republic of China; [2]State Key Laboratory of Powder Metallurgy and School of Materials Science and Engineering, Central South University, Changsha, Hunan, People's Republic of China

Introduction: Cancer is a major health problem worldwide, and the most extensive treatment can be obtained by using chemotherapy in the clinic. However, due to the low selectivity of cancer cells, chemotherapy drugs produce a series of grievous side effects on normal cells.

Methods: In this research, we developed novel nanocarriers for magnetically targeted near-infrared (NIR) light-electromagnetic wave dual controlled drug delivery based on $MgFe_2O_4$@CuS nanoparticles (NPs) modified with aminopropyltriethoxysilane (APTES) in response to magnetic, NIR light, and electromagnetic wave irradiation. Synthesis and characterization of $MgFe_2O_4$@CuS-APTES NPs was carried out using X-ray diffraction measurements, scanning electron microscopy, transmission electron microscopy, photoluminescence emission spectra, UV-1800 spectrophotometer, N5230A vector network analyzer, MDS-6 microwave sample preparation system, and superconducting quantum interference device. In addition to that mentioned above, we also explored many other sides, such as the drug-loading, drug-controlled release efficiency, elect99omagnetic wave thermal effect and photo-thermal effect.

Results: The results showed that APTES-modified $MgFe_2O_4$@CuS NPs had 37% high drug-loading capacity and high electromagnetic wave thermal conversion ability and NIR-light thermal conversion ability. In addition, ibuprofen (IBU) release from the $MgFe_2O_4$@CuS-APTES-IBU depends on the electromagnetic wave (2.45 GHz) and 1060 nm NIR light irradiation. After five cycles, the drug-release percentage was 90% and 66% separately, and could be adjusted by the time and cycles times of electromagnetic wave and NIR light irritation. Electromagnetic wave irradiation compared with NIR light irradiation, has a higher drug release rate and better penetration. Therefore, choosing different stimulation methods according to the treatment needs of the disease, we can achieve accurate personalized treatment of the disease.

Discussion: Our findings indicate that multifunctional APTES modified $MgFe_2O_4$@CuS NPs could be used for the first time as a new drug carrier for "location-timing-quantification" drug release with magnetic targeting and dual control of NIR light-electromagnetic waves.

Keywords: $MgFe_2O_4$@CuS, magnetic targeting, NIR light-electromagnetic wave heat conversion property, dual controlled release

Correspondence: Hongxia Peng
Tel/Fax +86-18975111023
Email penghongxia1@126.com

Jun Guo
Email 961009854@qq.com

Introduction

Controlling cancer has become one of the world's key health strategies. Currently, the most comprehensive treatment used clinically is chemotherapy. However, chemotherapeutic drugs are distributed throughout the body as the blood circulates,

submit your manuscript | www.dovepress.com
DovePress
http://doi.org/10.2147/IJN.S267614

and only a few drugs are concentrated in the tumor, making it difficult to reach the therapeutic concentration and kill cancer cells. Due to the low selectivity of cancer cells, these drugs produce a series of serious side effects on normal cells.[1] Whatis more, uncontrolled release of drugs have the potential to damage some organs, for example, in a short period of time, the drug that was quickly released, can attack the heart and even cause death.[2] Thus, there is a need for an innovative controlled drug-delivery system that avoids the serious toxic side effects and promotes improved patient compliance. The drug-delivery systems with "positioning, timing, and quantification" are controlled release technologies, and people have a keen interest in it in recent decades. It can improve the delivery efficiency of drugs to target site, reduce its toxicity, avoid first-pass effect, improve patient compliance, and prolong the duration of action by increasing drug content in tumor sites and regulating drug distribution in the body, thus reducing the frequency of drug administration.[2]

In the wake of developments in materials science and nanotechnology, various nanomaterials with "positioning, timing, and quantification" properties have become potential drug carriers for drug-delivery systems. In particular, inorganic nanomaterials, including magnetic nanoparticles and semiconductor nanoparticles have been extensively studied and used in the drug-delivery systems due to their magnetic, magneto-electric, and optical properties, and good biocompatibility. As an illustration, Kaushik et al[3] developed a ~20 nm, 10 mg/kg magnetoelectric nanocarrier (MENC) for noninvasive magnetic guided delivery across the blood–brain barrier of C57B1/J mice. MENCs were evenly distributed in the brain, were nontoxic to the brain and other major organs, at the same time, which had no impact on hepatic, kidney and neurobehavioral functioning. Kaushik et al[4] demonstrated that magnetic guided noninvasive delivery of a nanoformulation (NF), which consisted of Cas9/gRNA combined with magnetoelectric nanoparticles (MENPs), can inhibit the passage of potential HIV-1 infection in microglia (hμglia)/HIV (HC69) cells through the blood–brain barrier. The results showed that compared with unbound Cas9/g-RNA, developed NF remarkably reduced HIV-LTR expression in HIV latent hμglia/HIV (HC69) cells. Pandey et al[5] synthesized MENPs, which were composed of a piezoelectric shell and a ferromagnetic core, can exhibited enhanced cell uptake and controlled drug release due to the enhanced localized electric field (surface charge/potential), as well as the acoustics generated by the application of alternating current (AC) magnetic field (B) stimulation. The results confirmed that the local surface potential of MENP was enhanced by AC B-field (60 Oe) stimulation. A magnetically guided brain delivery method previously demonstrated in mice has not yet been translated for clinical applications due to the mismatch in the size and shape of available static magnets relative to human brains. Kaushik et al[6] explored magnetic resonance imaging (MRI) as a tool for delivering MENPs into the brain of a baboon, as a proof-of-concept study. MRI brain image analysis revealed reduced T_2 value at the basal ganglia, hemisphere, and vertex, thereby confirming successful MENP delivery to the brain.

$MgFe_2O_4$ NPs possess excellent chemical stability and stronger super-paramagnetic and electromagnetic wave absorption properties.[7] $MgFe_2O_4$ NPs which have magnetic-electromagnetic wave absorption properties, can be regarded as a magnetic target agent and electromagnetic wave thermal conversion agent for controlled-release drugs. As a drug carrier, $MgFe_2O_4$ NPs can be used for targeted drug delivery and tumor-targeted therapy. $MgFe_2O_4$NPs have excellent the electromagnetic wave heat conversion properties, and can generate controllable electromagnetic wave heating effect through complex phase dielectric loss.[8,9] It is worth paying more attention so that it would not cause skin effect at high frequency due to its high resistivity.[10] As drug carrier, it can avoid the overheating of surface and burning of biological tissue.[11] $MgFe_2O_4$ NPs are the first choice for medical high frequency electromagnetic wave absorbers. The electromagnetic wave has the advantages of rapid heating, high thermal efficiency, tissue penetration (up to 15 cm)[12,13] and controllability (changing electromagnetic wave power and radiation time), so it is noninvasive. It is not only suitable for the treatment of superficial tumors, but also for the treatment of deep organ tumors.

CuS nanocrystals are single near-infrared (NIR) photothermal agents with strong surface plasmon resonance (SPR), by activating an overburdened immune system, which can load and control the releasing tumor antigens in the tumor microenvironment as well as reactivate the ability of *T* cells to kill tumors.[14,15] At the same time, through its photothermal transformation, it can become a good drug carrier, loading and positioning, timing and quantitative release of anti-tumor drugs. Zhao et al designed and synthesized drug-loaded CuS nanocrystals for highly effective photo-thermotherapy of tumors guided by ultrasound imaging.[16] However, CuS nanocrystals as a

photo-thermal agent, are only suitable for superficial tumors by local heating of light, because they can erode epidermal tissue due to overheating and insufficient penetration. As a carrier, CuS nanocrystals still lack targeting.

In order to accumulate sufficient doses of anticancer drugs in tumor sites to kill cancer cells, payload anticancer drugs are one of the important research factors. The increase in drug loading rate usually requires more binding sites for the drug on the carrier. As drug carriers, inorganic nanoparticles must be endowed with surface activity by introducing organic functional groups to achieve high drug-loading efficiency. In general, carboxyl（-COOH）and amino（-NH_2）groups are introduced on the surface of inorganic nanoparticles, examples are polyacrylic acid, polylactic acid and polydopamine.[17,18] Aminopropyltriethoxysilane (APTES) has a surface functional group (-NH_2) and has good ability of chelating metal ions and can promote the drug loads onto the surface of the carrier, such as chemical bond or hydrogen bond, to improve the change of drug load rate in the external environment, these forces can be destroyed to achieve controlled release of the drug.[19,20]

Herein, we have prepared a new drug-delivery system with magnetic, NIR light and electromagnetic wave sensitivity combining the advantages of $MgFe_2O_4$ NPs and CuS nanocrystals with advantages of APTES, as shown in Figure 1. And the use of $MgFe_2O_4$@CuS-APTES NPs has not previously been reported for drug-delivery systems with "positioning, timing, and quantification". This new drug carrier has the following advantages. First, $MgFe_2O_4$ NPs core with magnetic properties can transport the drug to the target tissue under the external magnetic field, thus improving the treatment efficiency of the drug. Meanwhile, $MgFe_2O_4$ core also has the effect of heat transformation of electromagnetic wave, which realizes the controlled release of the drug. Second, the CuS nanocrystals achieve the drug controlled release due to NIR light thermal conversion effect. Third, APTES contains hydrogen bonded donor NH_2 that can load drugs through hydrogen bond interactions. $MgFe_2O_4$@CuS-APTES NPs as the carriers to controlled release ibuprofen (IBU) through electromagnetic wave and NIR light irradiation would be the most promising drug-delivery system with "positioning, timing, and quantification". This synergistic treatment strategy may provide new ideas for precise treatment of metastatic and recurrent tumors.

Experimental Sections

Magnesium sulphate ($MgSO_4 \cdot 7H_2O$,99.9%), cupric sulphate (purity ≥99.0%, $CuSO_4 \cdot 5H_2O$) and the APTES were purchased from the Shanghai Chemical Reagent Factory (Shanghai, China). IBU was purchased from the Jiangsu Hengrui Medicine Factory.

$MgFe_2O_4$ NPs were produced by the solvent-thermal method. Briefly, $FeCl_3 \cdot 6H_2O$ (1.352 g) and $MgSO_4 \cdot 7H_2O$ (0.845 g) were dissolved in ethylene glycol (40 mL) to make a clear solution, followed by the addition of NaAc (3.6 g) and polyethylene glycol (1.0 g). The mixture was stirred vigorously for 30 min, and then sealed in a teflon-lined stainless-steel autoclave (200 mL capacity). The autoclave was heated to 180°C and maintained for 12 h, and then left to cool naturally to room temperature. Wash The black products were washed several times with ethanol, which needed to be dried at 50°C for six hours finally. Then, the $MgFe_2O_4$ NPs were obtained.

A CuS nanocrystals was coated on the surface of $MgFe_2O_4$ NPs by the solvent-thermal method. In a typical procedure, $MgFe_2O_4$ NPs were prepared by 0.1g dispersed in 80 mL H_2O, and then $CuSO_4 \cdot 5H_2O$ (0.416, 1.248 and 2.48 g) and $Na_2S_2O_3 \cdot 5H_2O$ (2.48 g) were added. The solution was transfer into hydrothermal reactor and then maintained at 120, 150, and 180°C for six, eight, ten hours. Afterwards the $MgFe_2O_4$@CuS NPs were separated with a magnet, washed and dried.

We scattered 0.2 g $MgFe_2O_4$@CuS NPs into 4 mL ethanol and 40 mL H_2O. After stirring at room temperature for about 10 min, 2.5 mL APTES are added, and then heated to 80°C under intense mechanical stirring. After three hours the product was precipitated and washed with centrifugal water, and dried at 60°C overnight. The resulting products were $MgFe_2O_4$@CuS-APTES NPs.

We added 0.1 g of $MgFe_2O_4$@CuS-APTES NPs to 100 mL of deionized water-IBU solution with IBU concentration of 1 mg/mL^{-1} and stirred at room temperature for 12 h. At specified time points, the IBU loaded sample was magnetically collected and the characteristic IBU absorbance at 220 nm in the supernatant was measured using an UV−vis spectrophotometer.

$\text{Drugloading}(w/w\%) = M_{ads}/M_{add}$, where M_{ads} is the mass of drug adsorbed, and M_{add} is the mass of drug added during the loading process.[21]

IBU release was measured in five cycles of NIR light and electromagnetic wave radiation to check the controlled release characteristics of the drug. $MgFe_2O_4$@CuS-APTES-IBU (at 0.1 mg/mL 2 mL) in simulated body fluid (SBF) solution was exposed to five cycles of the NIR light and electromagnetic wave. In each cycle, the solution was irradiated for one minute, then turned off the NIR light and electromagnetic radiation. The

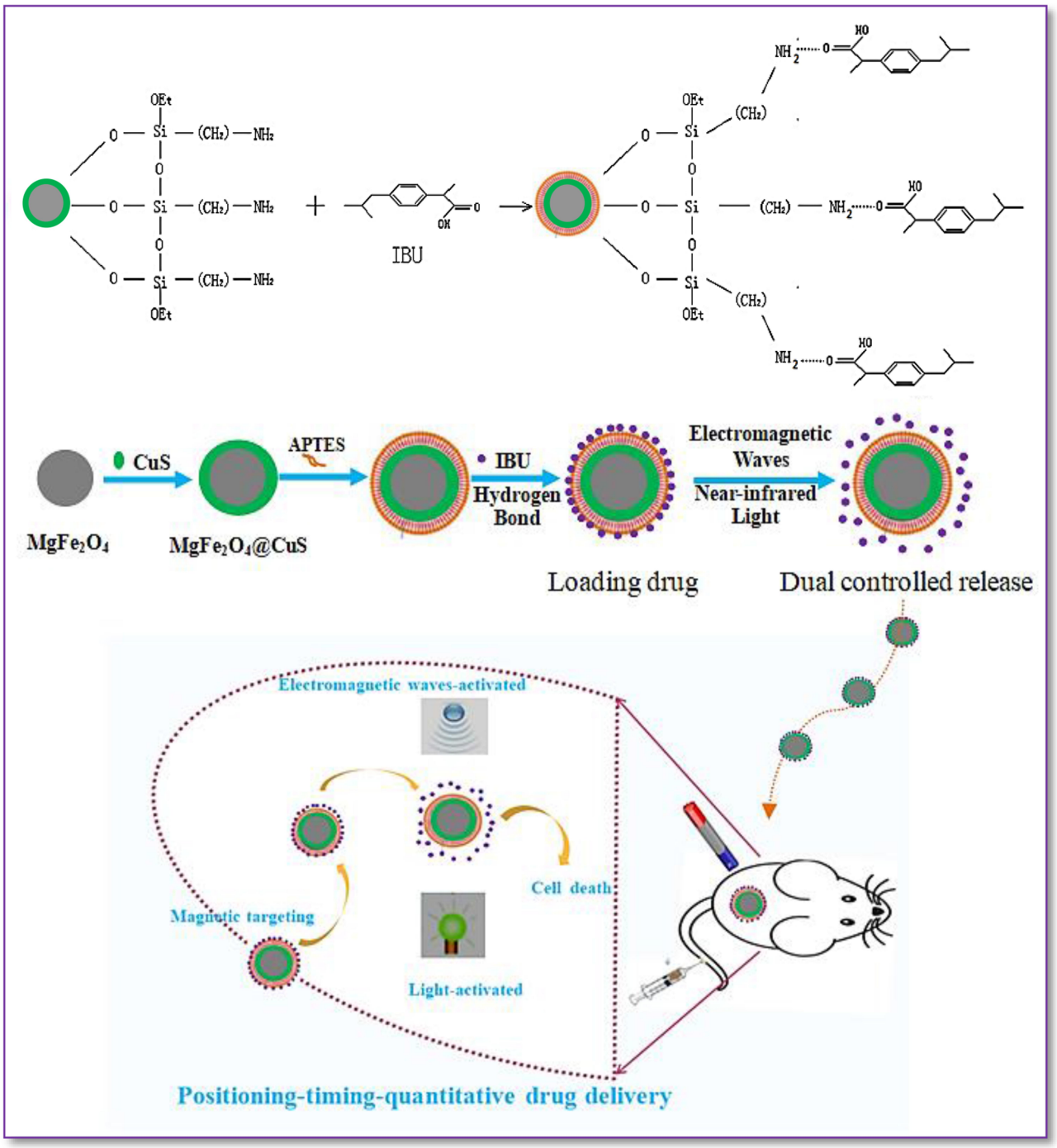

Figure 1 Schematic illustration of creating $MgFe_2O_4$@CuS-APTES NPs and the magnetic targeted delivery and dual controlled release of IBU by NIR light and electromagnetic waves.

solution was stored at room temperature for six hours and the UV-vis intensity of the solution was measured.

Drug releasing(w/w%) = M_{rel}/M_{ads}, where M_{res} is the amount of drug release, M_{ads} is the quality of adsorbed drug.

AXS D8 Advance Diffractometer was used to obtain X-ray diffraction (XRD) patterns. The morphology and structure of the samples were examined by a Philips XL30 ESEMFEG scanning electron microscope and transmission electron microscope (Hitachi, H-600).UV-1800 spectrophotometer was used to obtain Ultraviolet-visible light (UV–vis) spectral absorption values. Hitachi F-4500 spectrofluorimeter equipped with a 150 W xenon lamp as the excitation source for obtaining the photoluminescence (PL) emission spectra. The magnetic properties are examined using the

MPMS-XL-7 superconducting quantum interferometer (SQUID). MDS-6 microwave sample preparation system is used for controlled drug release via electromagnetic waves. Drug release was controlled by NIR light using a 1064 nm laser (FLIR A300). The electromagnetic parameters of $MgFe_2O_4$ and $MgFe_2O_4$@CuS NPs were obtained using the N5230A Vector Network Analyzer (Agilent). All of the measurements were performed at room temperature.

Results and Discussion

Structure and Morphology

As shown in Figure 2, we have successfully manufactured the composite materials consisting of $MgFe_2O_4$ (▲) NPs and CuS nanocrystals (Δ). In addition, there is no diffraction peak of the third phase material in the diffraction spectrum of composite materials, indicating that there is only physical interaction between $MgFe_2O_4$ NPs and CuS nanocrystals. At the same time, we have studied that different experimental conditions would have what kinds of effects on crystal structure. The diffraction peaks become higher at the different reaction temperature, indicating that the crystallinity of CuS nanocrystals will rise with the increasing of reaction temperature (Figure 2A). Figure 2B showed that the diffraction peaks become stronger and stronger, indicating that the crystallization growth of CuS nanocrystals will continue to occur on the surface of $MgFe_2O_4$ NPs with the prolongation of reaction time. Figure 2C showed that the higher the core:shell mass ratio is, the thicker the CuS nanocrystals are and the stronger the diffraction peak intensity are. The results showed that

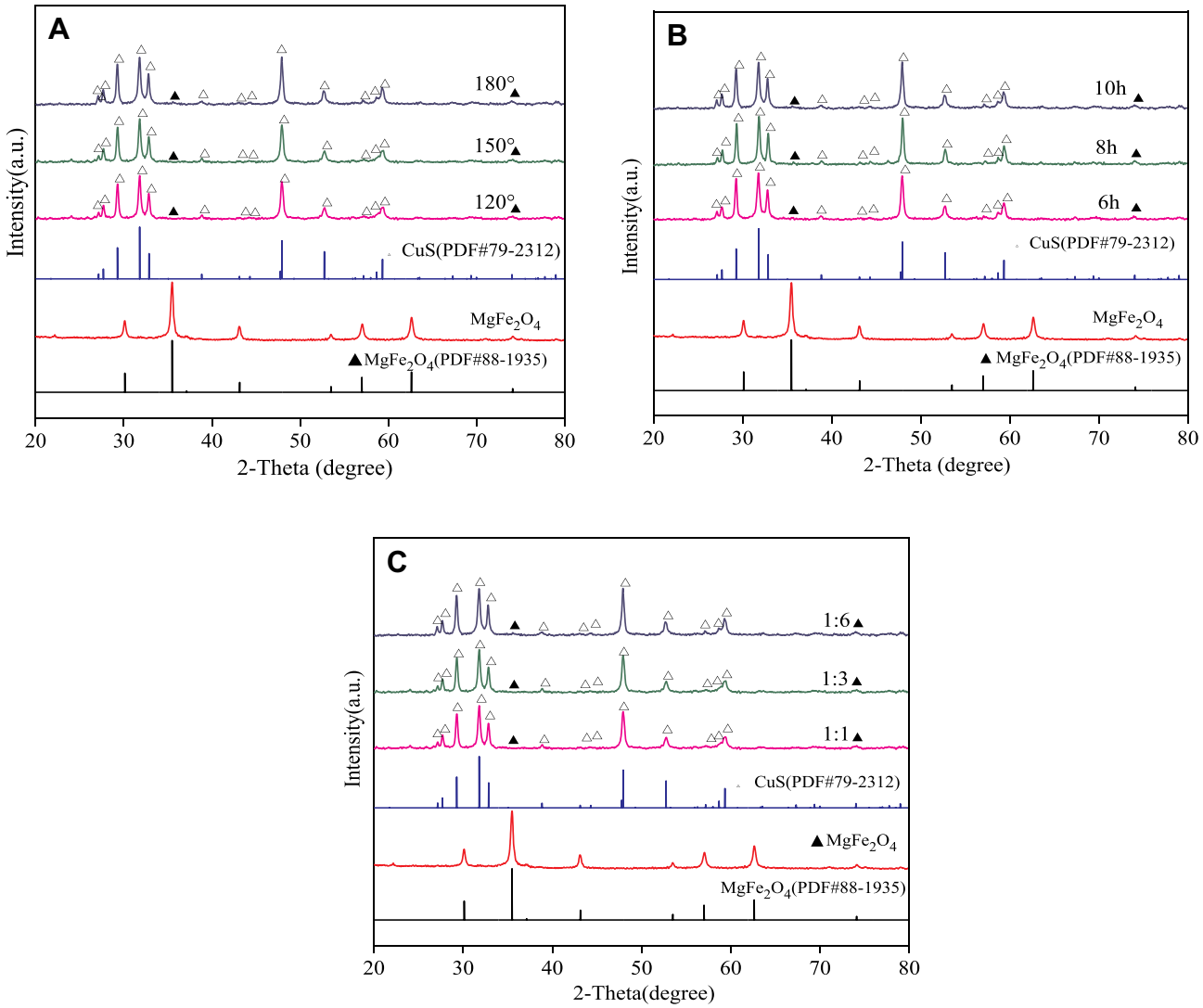

Figure 2 XRD patterns of $MgFe_2O_4$ (▲) and $MgFe_2O_4$@CuS NPs (Δ): (**A**) Different reaction temperature; (**B**) Different reaction time; (**C**) Different the mass ratio of core to shell.

different preparation conditions have great impact on the crystallinity and content of CuS nanocrystals.

We have researched the photoluminescence (PL) properties of $MgFe_2O_4$@CuS NPs for the purpose of looking into the effect of preparation conditions on the defect concentration of the CuS nanocrystals. The surface defect concentration of CuS nanocrystals can have influence on SPR effect of CuS and thus affect the NIR light thermal effect of $MgFe_2O_4$@CuS NPs. In general, the defects of CuS nanocrystals, as an illustration Cu vacancy, are common defects. They act as luminescent centers, emitting light through electron-hole recombination.[22] The luminescence property of CuS nanocrystals arises from surface defects, and the luminescence intensity of CuS nanocrystals is related to the defect density. Figure 3 showed emission bands of $MgFe_2O_4$@CuS NPs are all in the ultraviolet region. The purple emission band at 330–450 nm and the strong blue emission peak at 395 nm are attributed to surface defects of CuS nanocrystals.[23] As the reaction temperature increased from 120°C to 150°C, the luminescence intensity at 395 nm was attributed to the higher temperature, resulting in more defects of CuS nanocrystals. These defects enhanced the luminescence intensity of CuS nanocrystals, which indicated that the surface defect concentration of CuS nanocrystals is affected by the reaction temperature (Figure 3A). With the increase of reaction time from six to ten hours, fluorescence intensity of $MgFe_2O_4$@CuS NPs did not increase remarkably, because the range of reaction time from six h to ten hours had no significant effect on the number of surface

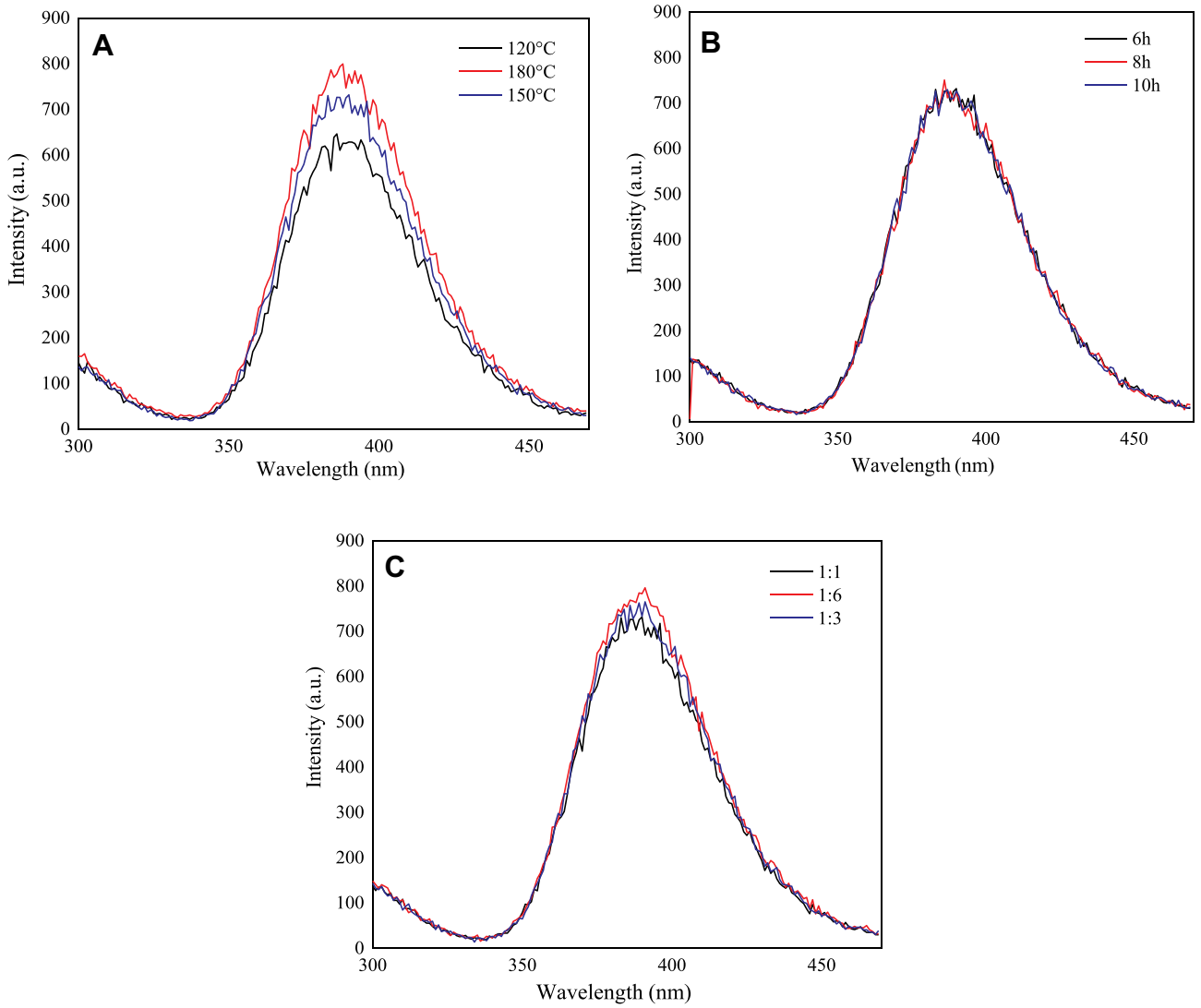

Figure 3 Fluorescence emission spectra of $MgFe_2O_4$@CuS NPs: (**A**) different reaction temperature; (**B**) different reaction time; (**C**) different the mass ratio of core to shell.

defects of CuS nanocrystal (Figure 3B). Figure 3C showed the higher the core:shell mass ratio is, the thicker the CuS nanocrystals are and the stronger the fluorescence intensity is. The results showed that the defect concentration of $MgFe_2O_4$@CuS NPs is affected by different preparation conditions and the NIR light thermal effect of $MgFe_2O_4$@CuS NPs are accurately under control of varying reaction temperature and the Cu content in the core-shell structure.

Since the morphology and properties of $MgFe_2O_4$@CuS NPs with the optimal defect concentration were studied, the defect concentration of CuS nanocrystals directly affected the SPR effect. In order to clarify the morphology of the $MgFe_2O_4$@CuS NPs, we obtained SEM images of the $MgFe_2O_4$ and $MgFe_2O_4$@CuS NPs (Figure 4). As can be seen from Figure 4A, C, E, $MgFe_2O_4$ NPs are a spherical particle of about 100 nm with good dispersibility. The $MgFe_2O_4$ NPs were composed of many $MgFe_2O_4$ nanocrystals and have a rough surface. Figure 4B, D, F shows that the $MgFe_2O_4$@CuS NPs still in spherical shape, but because CuS nanocrystals are deposited on the surface of $MgFe_2O_4$ NPs, its diameter is larger than $MgFe_2O_4$. The mean diameter of $MgFe_2O_4$@CuS NPs is around 300 nm and the surface is relatively smooth. In the $MgFe_2O_4$@CuS NPs, many CuS nanocrystals in the size range of 1–2 nm (Figure 4F) are uniformly coated on the $MgFe_2O_4$ NPs surface. The results showed that $MgFe_2O_4$@CuS NPs were obtained.

Figure 5A and B shows that the average particle size of $MgFe_2O_4$@CuS NPs is 300 nm and remains spherical without aggregation and rough surface. In the $MgFe_2O_4$@CuS NPs, many CuS nanocrystals in the 1–2 nm range are uniformly coated on the $MgFe_2O_4$ surface. Furthermore, the high resolution TEM image (Figure 5C) further confirmed the successful crystallization of CuS on $MgFe_2O_4$ surface. The lattice spacing on the surface is 0.32 nm, corresponding to the (110) plane of CuS, while 0.25 nm corresponds to the (311) plane of $MgFe_2O_4$. The results showed that the CuS layer is overlaid on $MgFe_2O_4$ NPs. Moreover, the shell thickness can be adjusted by changing the concentration of nitrate and the reaction time.

To further identify the structure of the $MgFe_2O_4$@CuS NPs, EDX mapping of the corresponding $MgFe_2O_4$@CuS was examined to analyze the elements, as shown in Figure 5. Figure 5D–I represent the mapping of Mg, Fe, O, Cu, S, and percentage content of each element, respectively. It can be seen that all the elements were distributed homogeneously in the sample. From EDX mapping and TEM, we can further confirm the formation of $MgFe_2O_4$@CuS NPs. Figure 5I shows that the electron beam cannot pass through the $MgFe_2O_4$@CuS NPs due to the thick CuS shell, so the percentage of Mg and Fe is lower, and therefore, the content of Cu and S in the outer layer is higher.

Magnetic Properties

The magnetic measurements showed that $MgFe_2O_4$ has magnetization saturation values of 49.87 emu g^{-1} (Figure 6). In compassion of a previous study in which $MgFe_2O_4$ NPs was synthesized by precipitation method,[24] the $MgFe_2O_4$ NPs exhibited stronger magnetic properties. The magnetization curves of $MgFe_2O_4$@CuS NPs are given in Figure 6. The value of saturation magnetization (*Ms*) is 10.01 emu/g for $MgFe_2O_4$@CuS NPs (Figure 6). It should be pointed out that $MgFe_2O_4$@CuS NPs retains stronger magnetic properties, indicating that it is suitable for magnetic targeting and separation as a drug carrier, which is smaller than that of the $MgFe_2O_4$ NPs due to the reduction in $MgFe_2O_4$ in the $MgFe_2O_4$@CuS NPs. The enlarged hysteresis loops (the inset graph in Figure 6) show that the remanent magnetization (*Mr*) of $MgFe_2O_4$ and $MgFe_2O_4$@CuS NPs were 3.58 and 0.14 emu g^{-1}, respectively. The coercivity (*Hc*) of $MgFe_2O_4$ and $MgFe_2O_4$@CuS NPs were 32.74 and 30.32 Oe (at 300 K), respectively. In addition, $MgFe_2O_4$@CuS NPs exhibits a fast response to external magnets, and it is prone to rapid redistribution after the removal of the magnetic field (Figure 6, inset). These results indicate that $MgFe_2O_4$@CuS NPs have magnetic responsivity and redispersibility, which is very important for practical operation.[25]

Electromagnetic Wave Absorption Properties and Electromagnetic Wave Thermal Conversion Effect

The frequency dependence on the relative dielectric constant of the $MgFe_2O_4$ and $MgFe_2O_4$@CuSNPs are shown in Figure 7. From the Figure 7A, we can observe that ε' values of $MgFe_2O_4$ and $MgFe_2O_4$@CuS NPs are about 6.1 and 3.5, respectively. Because the magnetic saturation strength of $MgFe_2O_4$ NPs is higher than that of $MgFe_2O_4$@CuS nanoparticles in magnetic field, the ε "value of $MgFe_2O_4$ NPs is higher than that of $MgFe_2O_4$@CuS NPs. Figure 7B showed that the ε"' values of$MgFe_2O_4$is greater than$MgFe_2O_4$@CuS NPs

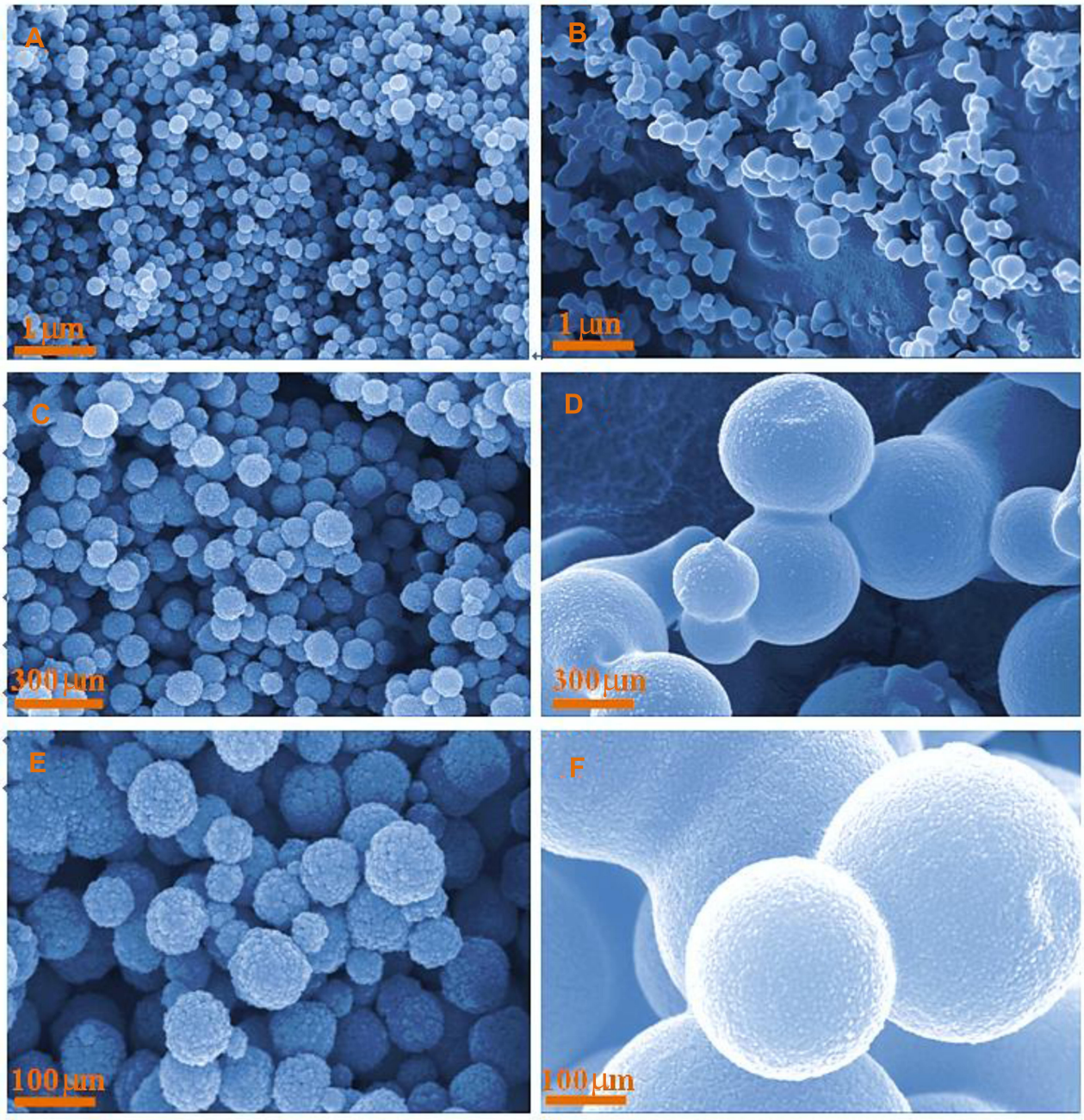

Figure 4 SEM of $MgFe_2O_4$ (**A, C, E**) and$MgFe_2O_4$@CuS (**B, D, F**) NPs.

and shows multiple relaxation peaks at different frequencies, respectively.

According to free-electron theory,[26] $\varepsilon'' = \frac{\sigma}{(2\pi f \varepsilon_0)}$, where σ is the conductivity, we found that $MgFe_2O_4$@CuS NPs has higher resistivity than the $MgFe_2O_4$. The real part μ' of relative permeability of the $MgFe_2O_4$ and $MgFe_2O_4$@CuS NPs varies with frequency and is shown in Figure 7C. The μ' values of $MgFe_2O_4$ and $MgFe_2O_4$@CuS NPs are in the range of 0.9–1.2, but μ' values of $MgFe_2O_4$ NPs show significant fluctuations. As can be seen from Figure 7D, the imaginary part μ'' of $MgFe_2O_4$ and $MgFe_2O_4$@CuS NPs relative permeability fluctuates significantly with the increase of frequency. In particular, the $MgFe_2O_4$ and $MgFe_2O_4$@CuS NPs shows distinct formant peaks at different frequencies.

The electromagnetic attenuation loss includes dielectric loss and magnetic loss. Dielectric loss tangent ($\tan\delta_e = \varepsilon''/\varepsilon'$) and magnetic loss tangent ($\tan\delta_m = \mu''/\mu'$)

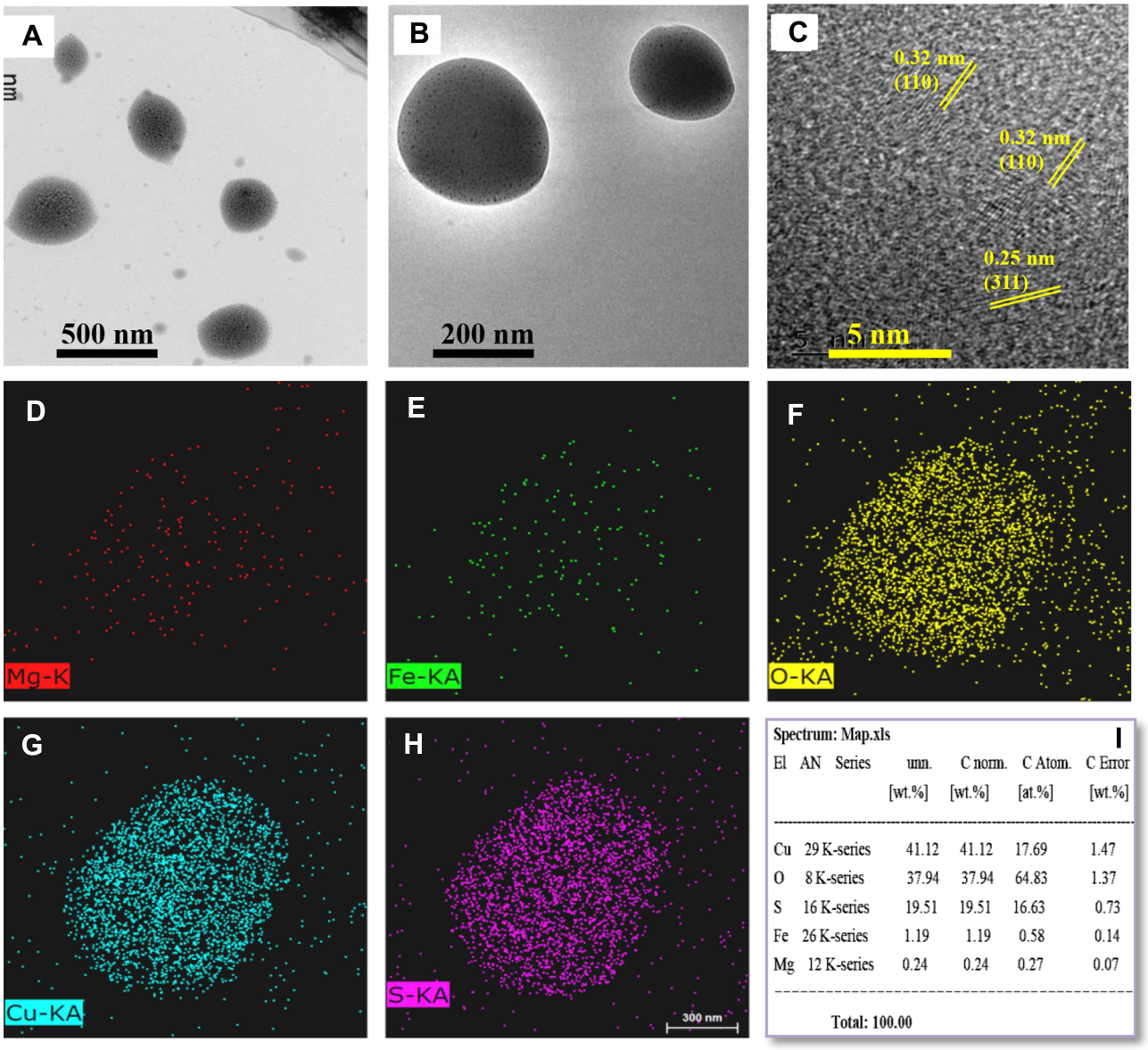

Figure 5 TEM (**A-C**) HRTEM images of $MgFe_2O_4$@CuS; (**D–I**) energy dispersive X-ray (EDX) mapping of $MgFe_2O_4$@CuS nanoparticles.

are extensively applied to evaluate the attenuation loss parameters, which have great impact on the electromagnetic wave absorption properties of electromagnetic wave absorption materials.[27] As shown in Figure 7E, what indicates $MgFe_2O_4$ NPs have a higher dielectric loss capacity is that the *tanδe* of $MgFe_2O_4$NPsis greater than $MgFe_2O_4$@CuS NPs. Figure 7F shows the *tanδm* values of $MgFe_2O_4$ and $MgFe_2O_4$@CuS NPs in the range 0–0.3. Furthermore, $MgFe_2O_4$ and $MgFe_2O_4$@CuS NPs show obvious magnetic loss peaks in tanδm~F curves. Moreover, what should be pointed out is that the value of tanδm is greater than that of tanδe in 2–18 GHz, which indicates that magnetic loss is the main electromagnetic attenuation loss mechanism of $MgFe_2O_4$@CuS NPs.

The RL of electromagnetic radiation under normal incidence of the electromagnetic is proposed by:[28]

$$RL = 20\lg\left|\frac{Z-1}{Z-1}\right| \quad (1)$$

where, Z is the normalized impedance between input impedance Z_{in} of the monolayer absorber and the impedance of free space Z_0, and Z is expressed as

$$Z = \frac{Z_{in}}{Z_0}\sqrt{\frac{\mu}{\varepsilon}}\tanh\left(j\frac{2\pi d}{\lambda_0}\sqrt{\mu\varepsilon}\right) \quad (2)$$

Here, μ and ε represent the relative complex permittivity and the permeability of the composite medium,

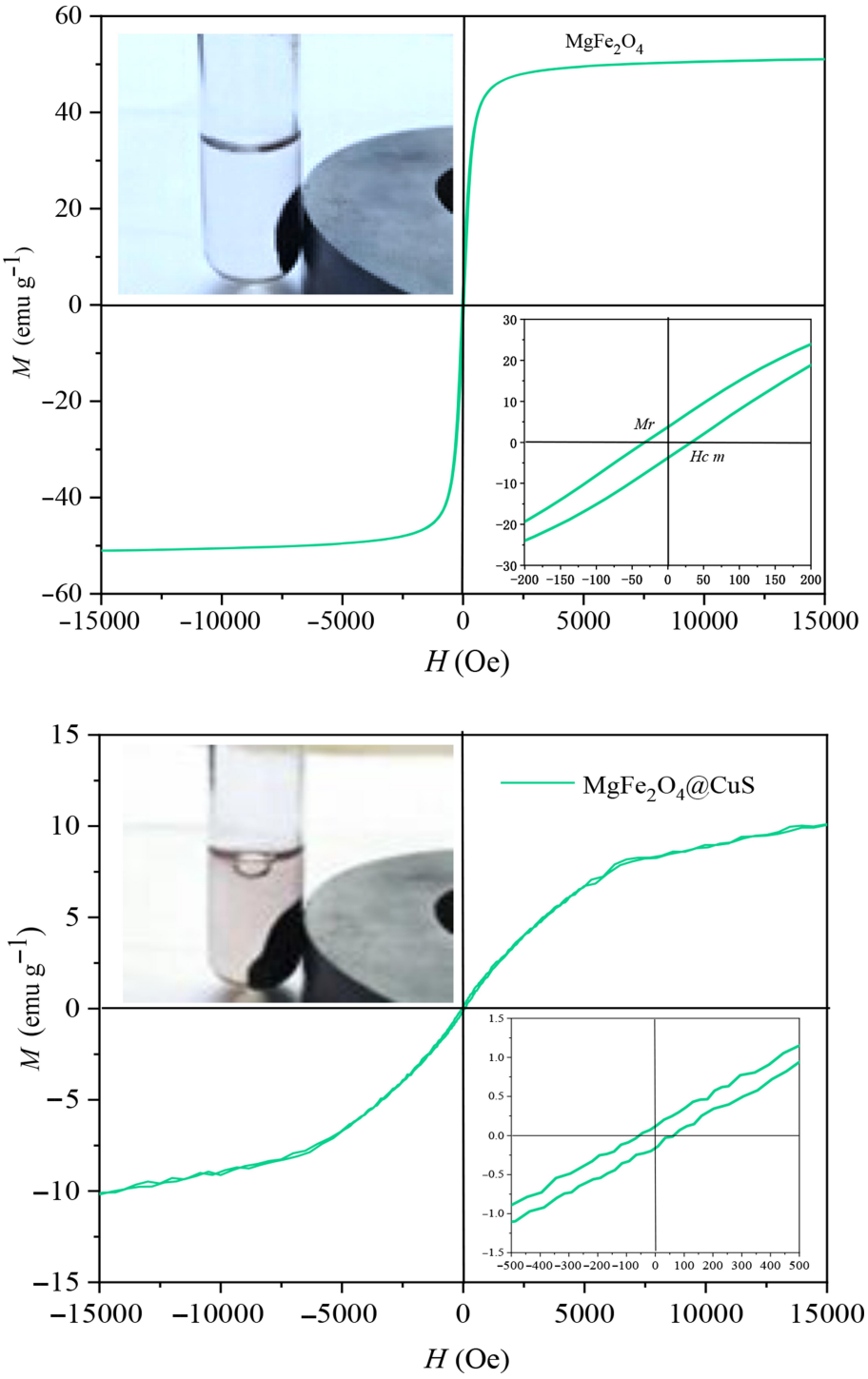

Figure 6 Magnetic hysteresis loops of $MgFe_2O_4$ and $MgFe_2O_4$@CuS NPs.

respectively, d is the thickness of an absorber, and λ_0 is the wavelength of the incident wave in free space. Therefore, the *RL* of an absorber is a function of six characteristic parameters, ε', ε'', μ', μ'', f and d. The electromagnetic wave absorption characteristics of NPs were calculated by computer simulation. The different measured values obtained previously were calculated using (1), such as ε', ε'', μ', μ''.

The calculated *RL* as a function of frequency for the samples are shown in Figure 8. It can be seen from Figure 8A and B that $MgFe_2O_4$ and $MgFe_2O_4$@CuS NPs have better electromagnetic wave absorption

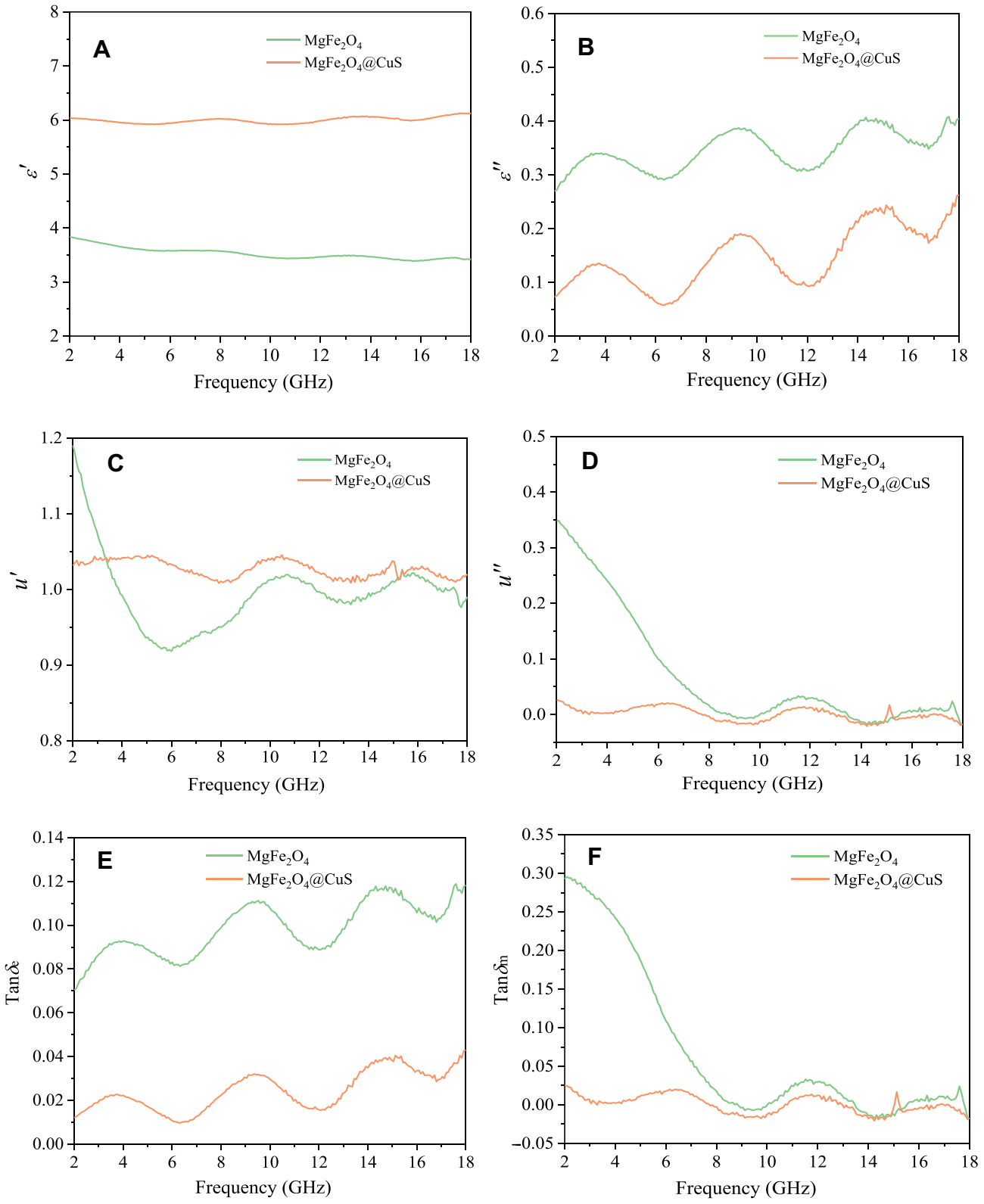

Figure 7 Frequency dependence of (**A**) ε', (**B**) ε'', (**C**) μ', (**D**) μ'', (**E**) tanδe and (**F**) tanδmfor the $MgFe_2O_4$ and $MgFe_2O_4$@CuS NPs.

property. The time–temperature curves of sodium chloride solution, $MgFe_2O_4$ and $MgFe_2O_4$@CuS NPs under electromagnetic wave irradiation are shown in Figure 8C. The reason why using $MgFe_2O_4$@CuS NPs for positioning-timing-quantitative drug release is that the $MgFe_2O_4$@CuS NPs have a good heating

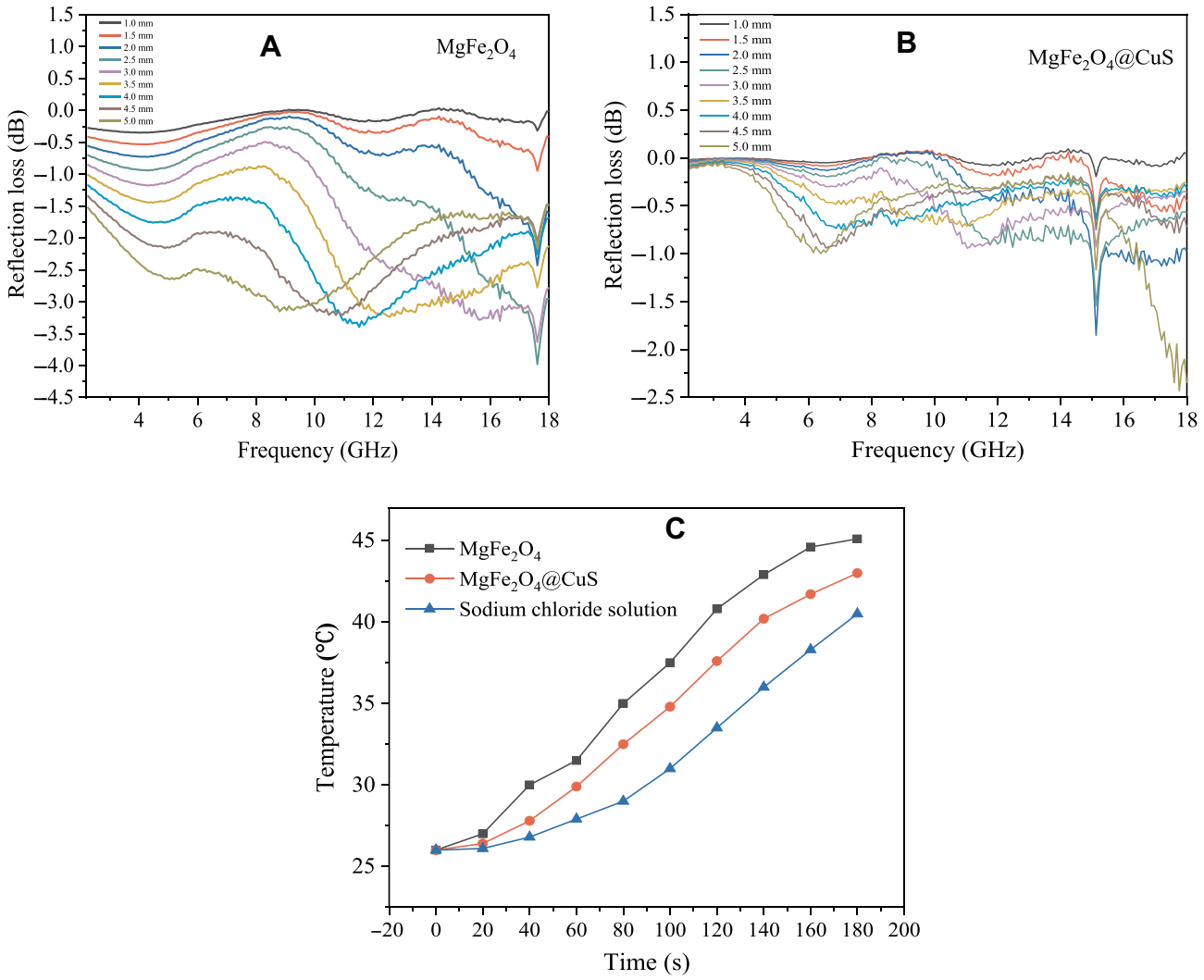

Figure 8 Frequency dependence of reflection loss with different thicknesses: (**A**) $MgFe_2O_4$ NPs, (**B**) $MgFe_2O_4$@CuS NPs and (**C**) The electromagnetic wave thermal response of time-dependent temperature curve for the sodium chloride solution, $MgFe_2O_4$ and $MgFe_2O_4$@CuS NPs dispersed in sodium chloride solution with electromagnetic wave irradiation.

effect, the room temperature was 26°C and it can arrive at 43°C in three minutes. This temperature is enough to touch off the delivery of the drug. The results make us known that $MgFe_2O_4$@CuS NPs possess good electromagnetic wave absorption ability and electromagnetic wave thermal conversion effect. Ferroelectrics and dielectric $MgFe_2O_4$@CuS NPs will convert the absorbed electromagnetic waves to heat energy through electromagnetic energy loss, which leads to a temperature increase of aqueous solution containing $MgFe_2O_4$@CuS NPs.[29] It is suggested that $MgFe_2O_4$@CuS NPs were suitable for localized hyperthermia to controlled-release drug and treatment of cancers.

SPR and NIR Light Thermal Conversion Effect

CuS semiconductor materials have defective structures that cause surface charge carriers to migrate and form SPR effects similar to those on the surface of noble metal nanoparticles. When NIR light incident on the surface of CuS nanocrystals, the frequency of incident photon matches the overall vibration frequency of the transmitted electrons of CuS nanocrystals, and CuS nanocrystals will produce strong absorption of photon energy.[30] The absorption intensity and absorption wavelength of NIR light of CuS nanocrystals are mainly affected by the concentration of defect, and the defect structure of hole doping is easily formed in the preparation process, thus SPR effect is produced under

NIR light irradiation.[30] The absorption of SPR of CuS nanocrystals can dynamically adjust by doping due to its SPR is based on the plasma resonance absorption of defect concentration, so CuS nanocrystals have higher photothermal stability.

As can be seen from the curve of $MgFe_2O_4$ NPs (Figure 9A), no obvious absorption peak is observed at 400–1600 nm. However, the apparent absorption bands of $MgFe_2O_4$@CuS NPs are located at the visible region from band gap absorption and SPR absorption band of CuS nanocrystals from the 400 nm to 1600 nm. These results are consistent with the intrinsic optical properties of CuS reported in the literature, which are derived from the strong SPR absorption of CuS nanocrystals.[30] The SPR of CuS nanocrystals derives from the Cu vacancies. When light incident on the surface of CuS nanocrystals, CuS nanocrystals will produce plasmon resonance, which redistributes the electromagnetic field of CuS nanocrystals, therefore the light is converted into heat energy, which produces the thermal conversion effect. The thermal conversion efficiency of $MgFe_2O_4$@CuS NPs is derived from the thermal conversion efficiency of CuS nanocrystals.[31]

The light thermal conversion performances of these $MgFe_2O_4$@CuS NPs were measured in aqueous dispersions with various concentrations (0, 50, 100, 200, and 400 μg/mL) radiated by a 1064 nm laser for five minutes at an intensity of 2 W/cm^{-2}. Figure 9B shows the temperature change curves. The pure water (0 μg/mL) displayed a slight temperature increase. However, the temperature of $MgFe_2O_4$@CuS NPs aqueous solution showed a significant increase under the same condition. The temperature increased to 33.3°C at a concentration of 100 μg/mL after five minutes of irradiation.

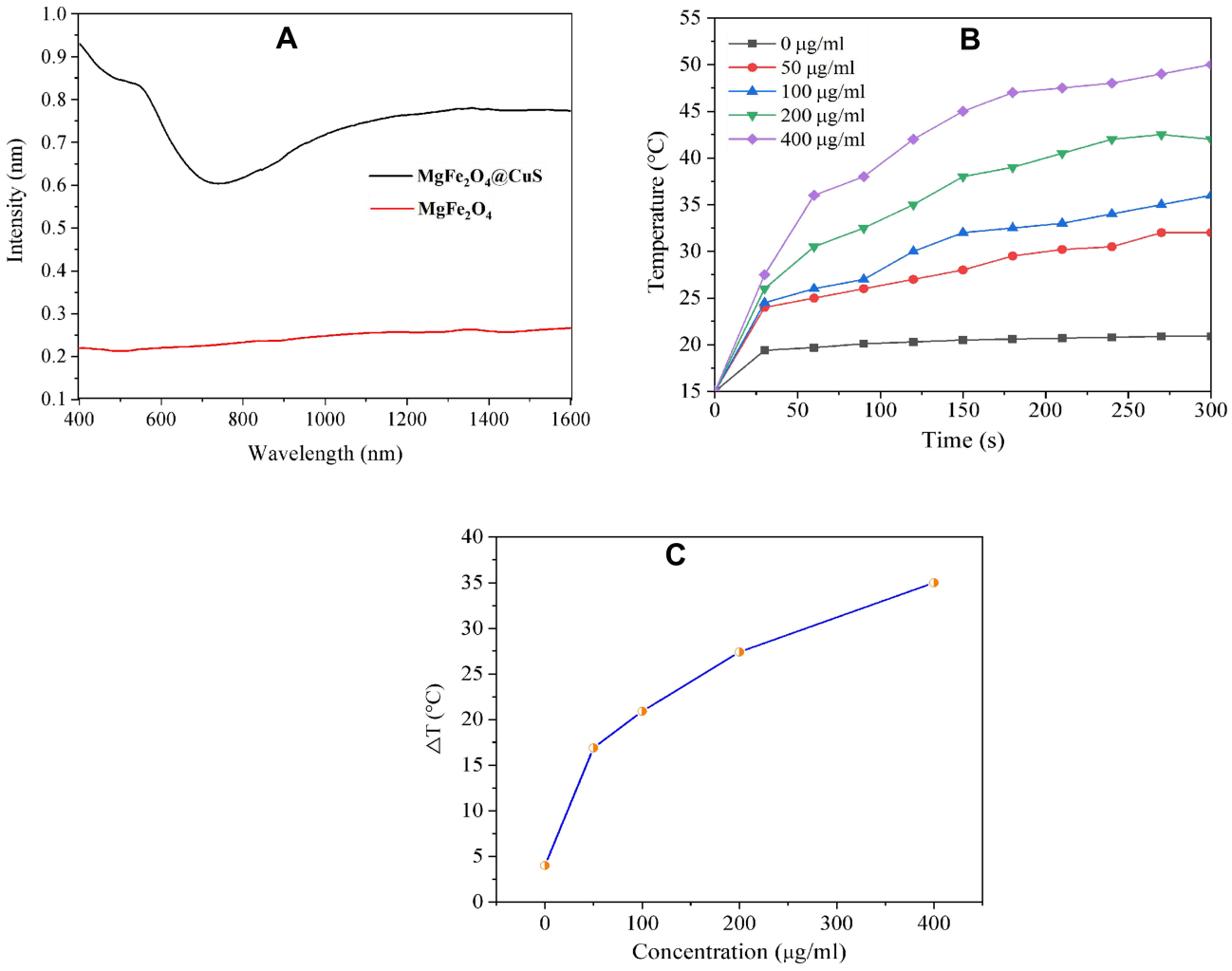

Figure 9 (**A**) UV–Vis–NIR absorption spectra of $MgFe_2O_4$ and $MgFe_2O_4$@CuS NPs; (**B**) Temperature elevation curves of aqueous dispersions containing $MgFe_2O_4$@CuS NPs with different concentrations under laser irradiation (1060 nm) with power density of 2 W cm^{-2}. (**C**) The concentration-dependent temperature difference curve of aqueous dispersions containing $MgFe_2O_4$@CuS NPs with different concentrations under laser irradiation.

When the concentration increased to 400 μg/mL, the temperature increased to 50°C. In contrast, the temperature of distilled water only increased by to 19°C. It was found that the temperature rise of these dispersion was directly proportional to the concentration of $MgFe_2O_4$@CuS NPs (Figure 9C). As shown in Figure 9C, the temperature of pure distilled water was only 4.0°C higher than that of the ambient (15°C), whereas $MgFe_2O_4$@CuS NPs aqueous solution at different concentrations was irradiated for five minutes, $MgFe_2O_4$@CuS NPs were found to be able to convert laser energy into heat, which increased by 16.9°C, 20.9°C, 27.4°C and 35.0°C, respectively.

Compared with a previous study in which Fe_3O_4@CuS microspheres,[32] the $MgFe_2O_4$@CuS NPs exhibited superior photothermal conversation property, since $MgFe_2O_4$@CuS NPs is more suitable for photothermal therapy. Compared with 980 nm, the energy loss at 1060 nm excitation wavelength caused by scattering and biotissue absorption is smaller.[33]

Drug Loading

The FT-IR spectra of$MgFe_2O_4$@CuS-APTES, $MgFe_2O_4$@CuS-APTES-IBU and pure IBU are given in Figure 10. From the Figure 10A, we can see that there are absorptions at 455–700 cm^{-1}, which can be allocated to the tensile vibration of Fe-O, Mg-O and Cu-S. Likewise, the bands $\nu(H_2O)$ at 3430 cm^{-1} proves the existence of adsorbed water molecules. In order to highlight characteristics that appear after modification by APTES, the vibration of Si atoms involved in siloxane and uncondensed organosilicon groups is distributed in the range of 900–1300 cm^{-1} wave number.[34] More precisely, the band at 1000 cm^{-1} is assigned to Si−O−Si and that at 1190 cm^{-1} to Si−O−C.[34] The band at 1190 cm^{-1} could also be due to Si−O−Cu groups, which would prove the covalent interaction.[34] However, we suggest that both Si−O−C and Si−O−Cu vibrations are associated with this absorption. Typical vibrations of alkyl groups are located at 2930 cm^{-1}.[34] An absorption band centered at 1597 cm^{-1} is seen in the difference spectra of both kinds of particles, which may be attributed to$\delta(NH_2)$,[34] which confirms the reactive NH_2 groups have been introduced at the surface of the $MgFe_2O_4$@CuS NPs. For IBU loaded $MgFe_2O_4$@CuS-APTES-IBU (Figure 10B), the band assigned to C=O (1720 cm^{-1}) is apparent, except that the strength decreased slightly compared with pure IBU (Figure 10C), confirming the successful incorporation of IBU onto the surface of the $MgFe_2O_4$@CuS-APTES NPs.

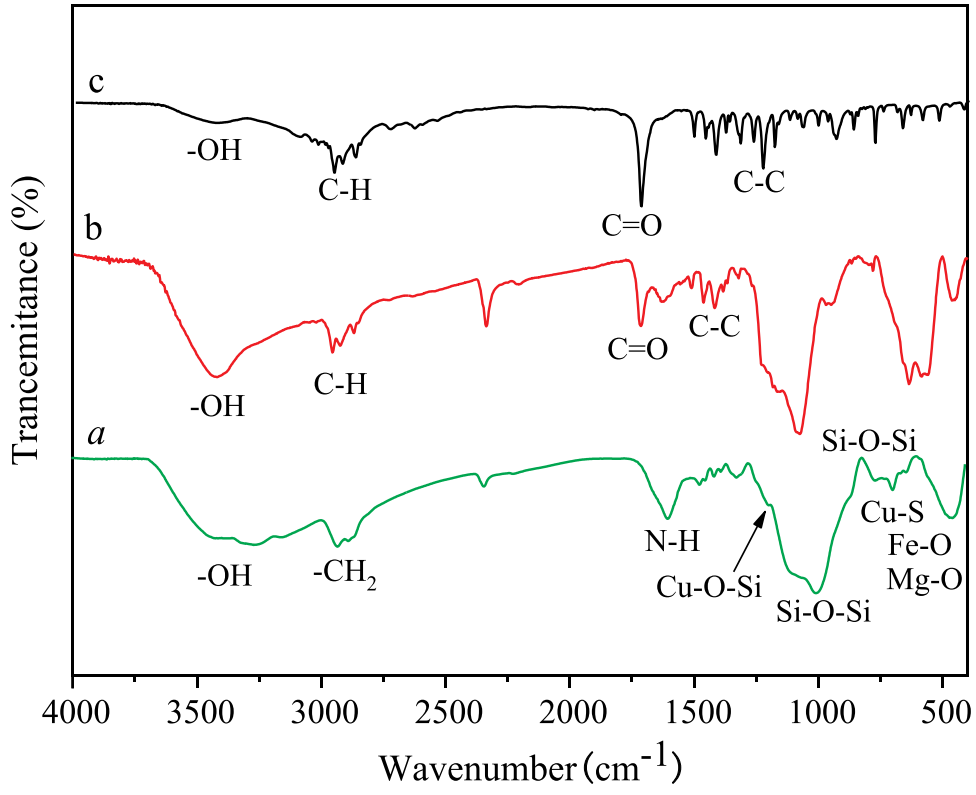

Figure 10 FTIR spectra of (**A**) $MgFe_2O_4$@CuS-APTES, (**B**) $MgFe_2O_4$@CuS-APTES-IBUand (**C**) pure IBU.

To study the drug storage and release properties of $MgFe_2O_4$@CuS-APTES NPs, IBU was selected as the model drug due to IBU (4-isobutyl-alpha-methylphenylacetic acid) contains the hydrogen bond receptor C=O.[35] The synthesized $MgFe_2O_4$@CuSNP shave been modified by reaction with APTES, to introduce hydrogen bonded donor NH_2 at their surfaces. Therefore, IBU was absorbed onto the surface of $MgFe_2O_4$@CuS-APTES NPs by forming hydrogen bond with amino groups of $MgFe_2O_4$@CuS-APTES. The hydrogen bond interactions remained stable at physiological temperature and are destroyed by heating. Figure 1 shows a diagram of loading IBU onto $MgFe_2O_4$@CuS-APTES NPs as a drug carrier by forming $MgFe_2O_4$@CuS-APTES-IBU NPs. Loading efficiency of IBU-loaded $MgFe_2O_4$@CuS-APTES NPs were evaluated and calculated.

Figure 11 indicates the change in drug loading rate vs time (room temperature, pH=7). In the first six hours, the drug loading rate was as high as 37%. The intensity of the absorption peak at 220 nm decreased over time (Figure 11A), indicating that the drug load was increasing. At 6–12 h, the absorption peak at 220 nm does not change, which indicates that the load is balanced. The results showed that 37% of IBU was adsorbed on the surface of $MgFe_2O_4$@CuS-APTES NPs (Figure 11B). This suggests the interaction between the amnio group of $MgFe_2O_4$@CuS-APTES and the carboxy group of IBU, thus increasing the IBU loading per surface area.

Drug Release

Figure 12 shows the IBU release process in vitro under moderate agitation in SBF medium, with immersion temperature maintained at 37°C (pH=6). The release of drug molecules depended on the pH of the medium and release time. Protonation of the drug (dissociation of $MgFe_2O_4$@CuS-IBU NPs) occurred at a lower pH, which released drug molecules into the medium. Rapid release from NP can be seen at the outset (25% of drugs are released within six hours). Then a gradual release of IBU molecules was measured, and approximately 40% of the adsorbed IBU has been released within 36 h (Figure 12B). The release remained almost constant over time, as confirmed by the invariant UV-Vis spectrum (Figure 12A). However, in a short period of time, the drug that was quickly released can attack the heart and even lead to death.[36] Controlled drug-release systems allow for controlling drug release with "positioning, timing, and quantification". Thus, controlled drug-release systems can decrease its side effects. The APTES modified $MgFe_2O_4$@CuS NPs may be a drug-delivery carrier to control drug release efficiency during disease treatment.

In order to confirm the IBU radiated by NIR light and electromagnetic wave irradiation, we carried out the drug release experiments without NIR light and electromagnetic wave irradiation. Figure 13 shows that the UV–vis absorption intensity of the irradiated solution was higher than that of nonirradiated solution over the whole wavelength range. This suggests that when irradiated with NIR light and electromagnetic waves, the hydrogen bond interaction between the $MgFe_2O_4$@CuS-APTES and IBU may be greatly weakened, thereby releasing the IBU. And the result also indicates that structural integration of released IBU is not changed due to the functional groups of IBU detected in the solution.

In order to estimate the controllability of the drug release of carrier, the carrier was treated with the NIR light and electromagnetic wave irradiation. For each cycle, the carrier was treated by NIR light and electromagnetic wave separately for one minute and NIR light and electromagnetic wave radiation were turned off for one hour. Figure 14 (green curve) demonstrates that the irradiation of electromagnetic wave can promote the release of IBU molecules and when electromagnetic waves are turned off, the release of IBU molecules is inhibited. About 11% of IBU molecules in$MgFe_2O_4$@CuS-APTES-IBU are released within one minute of the first exposure, one hour higher than that of IBU molecules without electromagnetic radiation, and only 2% of IBU molecules were released. Then a quick release of IBU molecules was measured, and about 60% of the adsorbed IBU has been released within two minutes. After five cycles about 90% of the IBU is released.The results show that the interaction force between the carriers and drug could be weakened by electromagnetic wave thermal conversion effect, thus IBU can be released. Compared with a previous study in which CuS/carbon dots nanocomposites,[37] the $MgFe_2O_4$@CuS NPs not only have superior photothermal conversion properties but also have good magnetic and electromagnetic wave conversion properties, since $MgFe_2O_4$@CuS NPs is more suitable for controlled release drug with "positioning, timing, and quantification" to improve the therapeutic effect of tumor.

Figure 14 (purple curve) indicates that NIR irradiation can promote the release of IBU. IBU release will stop when NIR radiation is turned off. About 10% of IBU was released

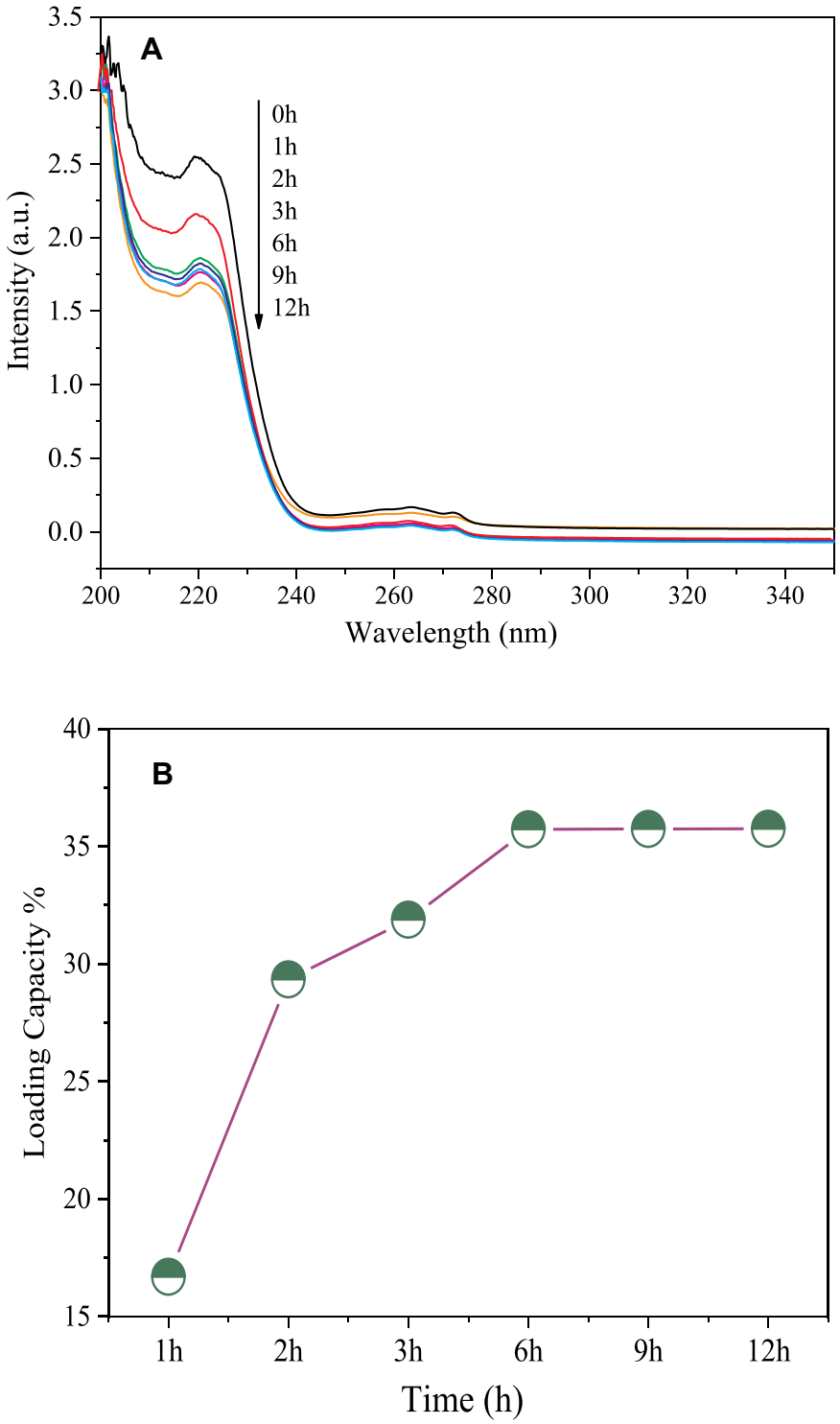

Figure 11 Drug loading behavior: (**A**) UV-vis spectra and (**B**) drug loading vs time.

on the first exposure of one minute of $MgFe_2O_4$@CuS-APTES-IBU, which was higher than that without NIR irradiation, only 2% od IBU molecules were released in one hour. Then about 66% of the adsorbed IBU was released within five minutes. The result showed that the IBU release was promoted by NIR light destroying the interaction between $MgFe_2O_4$@CuS-APTES and IBU. When the drug carrier was irradiated by electromagnetic wave and NIR light, they transformed heat through the thermal effect. Then temperature change destroys the interaction between

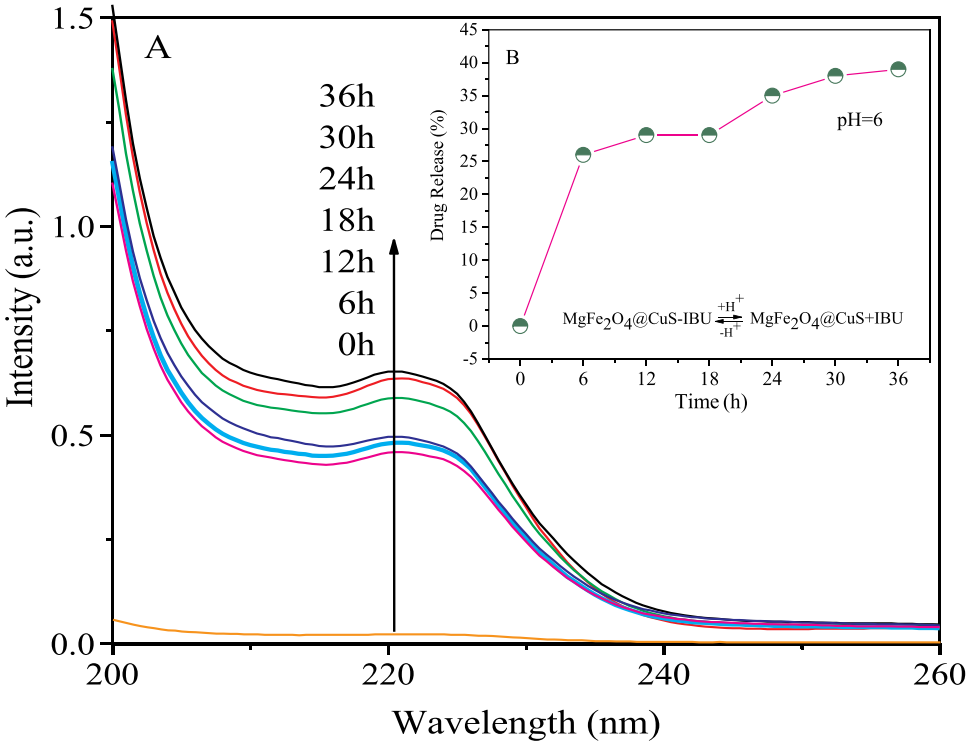

Figure 12 In vitro IBU release behavior at pH 6.0: (**A**) UV-vis spectra and (**B**) drug releasing vs time.

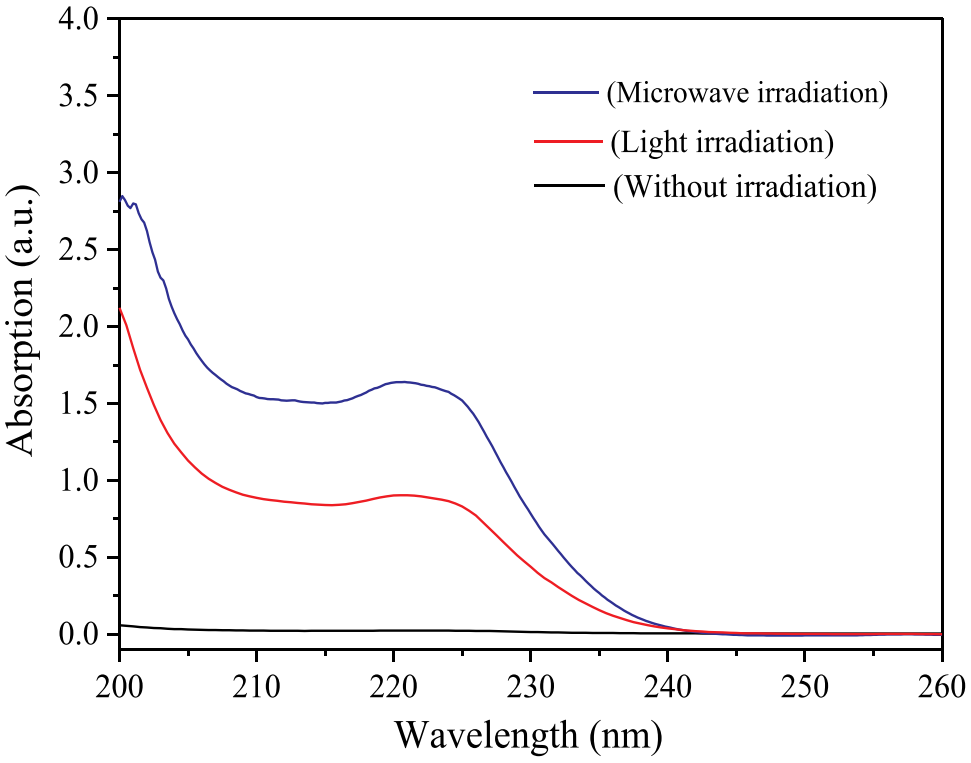

Figure 13 UV–vis absorption by the control group without illumination and the supernatant of samples irradiated for 2 minutes.

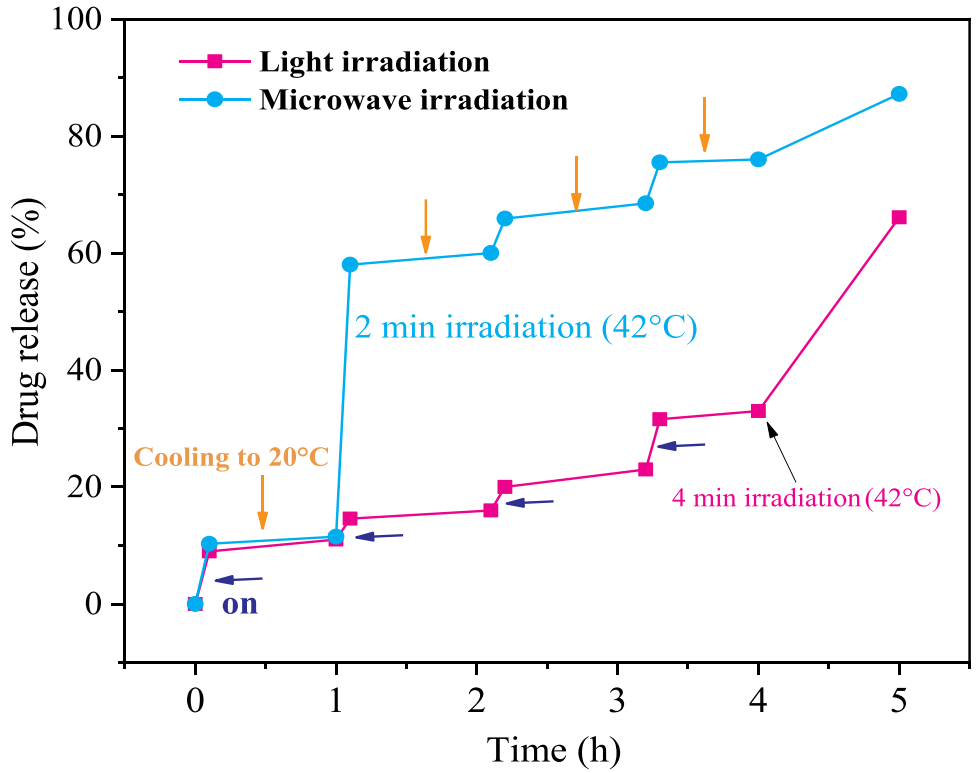

Figure 14 Controlled release profile of $MgFe_2O_4$@CuS-APTES-IBU under electromagnetic wave and NIR light irradiation.

IBU and $MgFe_2O_4$@CuS-APTES, thus controlling IBU release. The results showed that $MgFe_2O_4$@CuS-APTES-IBU NPs had good sustained and controlled release properties. Compared to previous studies (such as) $CoFe_2O_4$ microspheres[38] by microwave trigger controlled drug-delivery system, $MgFe_2O_4$@CuS NPs cannot only have excellent magnetic and electromagnetic wave dialogue performance, but also have good thermal performance dialogue, since $MgFe_2O_4$@CuS NPs are more suitable for magnetic targeted temperature sensitive controlled drug-delivery systems to improve the treatment effect of the tumor. Whatis more, the drug (IBU) in $MgFe_2O_4$@CuS-APTES-IBU NPs is released faster by electromagnetic wave irradiation than by NIR light irradiation and better penetration. Therefore we can choose different stimulation methods according to the treatment needs of the disease, so as to realize the precise and personalized treatment of the disease.

Conclusion

In this study, we successfully fabricated multifunctional APTES modified $MgFe_2O_4$@CuS NPs for magnetic targeting and dual control of drug release by NIR light-electromagnetic wave for the first time. Owing to the special structure of APTES and the versatility of $MgFe_2O_4$@CuS NPs, $MgFe_2O_4$@CuS-APTES NPs can load IBU and positioning-timing-quantitative release IBU. NIR light and electromagnetic wave stimulation successfully enhanced drug release from $MgFe_2O_4$@CuS-APTES NPs. Compared with NIR light irradiation, electromagnetic wave irradiation has a higher drug release rate and better penetration.

Challenges and Future

This study was a primary exploration of the synthesis and performance evaluation of $MgFe_2O_4$@CuS-APTES NPs. Further studies are needed to optimize the formulation and adjust the size and properties of $MgFe_2O_4$@CuS-APTES NPs for clinical research. More importantly, using live mice as animal models, the dispersibility, heat transfer efficiency and the controlled release effect of $MgFe_2O_4$@CuS-APTES-IBU NPs should be studied in vivo, and the effect of $MgFe_2O_4$@CuS-APTES NPs on the tissues and organs of live mice should be further studied. And $MgFe_2O_4$@CuS-APTES-IBU NPs should be confirmed in vivo as drug-delivery carriers before clinical application, to provide experimental and theoretical basis for clinical research.

Ethical Statement

Our study did not require an ethical board approval because it did not contain human or animal trials.

Funding

This work was supported by National Natural Science Foundation of China (grant number 51704116); Hunan Province Natural Science Foundation of China (grant numbers 2018JJ3252; 2017JJ3123); the scientific research project of Hunan Province, Department of Education (grant numbers 19A264; 18B457; 18C0886); the planned science and technology project of Hunan Province, China (grant number 2016TP1028); the double first-class discipline construction program of Hunan Province and China postdoctoral science foundation (grant number 2017M 612582).

Disclosure

The authors report no conflicts of interest in this work.

References

1. Huang SS, Ma PA, Wei Y. Controllable synthesis of hollow porous silica nanotubes/CuS nanoplatform for targeted chemo-photothermal therapy. *Sci China Mater*. 2020;63(5):864–875. doi:10.1007/s40843-019-1235-1
2. Yang X, He DG, He XX. Synthesis of hollow mesoporous silica nanorods with controllable aspect ratios for intracellular triggered drug release in cancer cells. *ACS Appl Mater Interfaces*. 2016;8(32):20558–20569. doi:10.1021/acsami.6b05065
3. Kaushik A, Jayant RD, Nikkhah-Moshaie R. Magnetically guided central nervous system delivery and toxicity evaluation of magneto-electric nanocarriers. *Sci Rep*. 2016;25309:6–13.
4. Kaushik A, Yndart A, Atluri V. Magnetically guided non-invasive CRISPR-Cas9/gRNA delivery across blood-brain barrier to eradicate latent HIV-1 infection. *Sci Rep*. 2019;3928:9.
5. Pandey P, Ghimire G, Garcia J. Single-entity approach to investigate surface charge enhancement in magnetoelectric nanoparticles induced by AC magnetic field stimulation. *ACS Sens*. 2020. doi:10.1021/acssensors.0c00664
6. Kaushik A, Rodriguez J, Rothen D. MRI-guided, noninvasive delivery of magneto-electric drug nanocarriers to the brain in a nonhuman primate. *ACS Appl Bio Mater*. 2019;2(11):4826–4836.
7. Chen P, Cui B, Cui X, Zhao W, Bu Y, Wang Y. A electromagnetic wave –triggeredcontrollabledrugdeliverysystembasedonhollow-mesoporous cobalt ferrite magnetic nanoparticles. *J Alloys Compd*. 2017;699:526–533.
8. Kubota M, Kanazawa Y, Nasu K. Effect of heat treatment on magnetic $MgFe_2O_4$ nanoparticles. *J Therm Anal Calorim*. 2008;92(2):461–468. doi:10.1007/s10973-007-8971-1
9. Kumar S, Daverey A, Sahu NK. In vitro evaluation of PEG-ylated-mesoporous $MgFe_2O_4$ magnetic nanoassemblies (MMNs) for chemo-thermal therapy. *J Mater Chem B*. 2013;1:3652–3660. doi:10.1039/c3tb20429d
10. Zhang L, Zhou XY, Guo XJ. Investigation on the degradation of acid fuchsin induced oxidation by $MgFe_2O_4$ under electromagnetic wave irradiation. *J Mol Catal A Chem*. 2011;335(1–2):31–37. doi:10.1016/j.molcata.2010.11.007
11. Chen W, Liu QY, Zhu XX. One-step in situ growth of magnesium ferrite nanorods on graphene and their electromagnetic wave -absorbing properties. *Appl Organomet Chem*. 2018;32(2):4017–4023. doi:10.1002/aoc.4017
12. Gao J, Yang SG, Li N. Rapid degradation of azo dye Direct Black BN by magnetic $MgFe_2O_4$-SiC under electromagnetic wave radiation. *Appl Surf Sci*. 2016;379(30):140–149. doi:10.1016/j.apsusc.2016.04.041
13. Korkusuz H, Happel C, Heck K. Percutaneous thermal electromagnetic wave ablation of thyroid nodules, preparation, feasibility, efficiency. *J Nuklearmedizin*. 2014;53(4):123–130. doi:10.3413/Nukmed-0631-13-10
14. Jiang M, Liu H, Zeng S, Hao J. A general in situ growth strategy of designing theranostic $NaLnF_4@Cu_{2-x}S$ nanoplatform for in vivo NIR-II optical imaging beyond 1500 nm and photothermal therapy. *J Adv Therap*. 2019;2:1800153–1800161. doi:10.1002/adtp.201800153
15. Bi H, Dai Y, Lv R, et al. Doxorubicin-conjugated CuSnanoparticles for efficient synergistic therapy triggered by near-infrared light. *Dalton T*. 2016;45:5101–5110.
16. Zhao Z, Wang S, Zhang S, et al. Targeted delivery of CuSnanoparticles through ultrasound image-guided microbubble destruction for efficient photothermal therapy. *Nanoscale*. 2013;5:3216–3219. doi:10.1039/c3nr00541k
17. Sperling RA, Parak WJ. Surface modification, functionalization and bioconjugation of colloidal inorganic nanoparticles. *Philos Trans A Math Phys Eng Sci*. 2010;368(1915):1333–1383.
18. Wang JX, Zhou HJ, Guo GY. A functionalized surface modification with vanadium nanoparticles of various valences against implant-associated blood stream infection. *Int J Nanomed*. 2017;12:3121–3136. doi:10.2147/IJN.S129459
19. Ting BQ, Han JW, Jin GY. High density silanization of nano-silica particles using γ-aminopropyltriethoxysilane (APTES). *Appl Surf Sci*. 2015;351:646–654. doi:10.1016/j.apsusc.2015.05.174
20. Hao YC, Chen Y, Xia HP. Surface chemical functionalization of starch nanocrystals modified by 3-aminopropyl triethoxysilane. *Int J Biol Macromol*. 2019;126:987–993. doi:10.1016/j.ijbiomac.2018.12.200
21. Peng HX, Cui B, Li GM. A multifunctional β-CD-modified Fe_3O_4@ZnO:Er^{3+}, Yb^{3+}nanocarrier for antitumor drug delivery and electromagnetic wave-triggered drug release. *J Mater Sci Eng C*. 2015;46:253–263. doi:10.1016/j.msec.2014.10.022
22. He J, Ai LS, Liu X. PlasmonicCuSnanodisk assembly based composite nanocapsules for NIR-laser-driven synergistic chemo-photothermal cancer therapy. *J Mater Chem B*. 2018;6(7):1035–1043. doi:10.1039/C7TB02772A
23. Hu C, Chen W, Xie Y. Generating plasmonic heterostructures by cation exchange and redox reactions of covellite CuS nanocrystals with Au^{3+} ions. *Nanoscale*. 2018;10(6):2781–2789. doi:10.1039/C7NR07283J
24. Heidari P, Masoudpanah SM. A facial synthesis of $MgFe_2O_4$/RGO nanocomposite powders as a high performance microwave absorber. *J Alloys Compd*. 2020;834:155166–155175. doi:10.1016/j.jallcom.2020.155166
25. Peng C, Wen JL, Jun LJ. Syntheses and magnetic properties of spinel-type MFe_2O_4 (M=Ca, Mg, Cu, Zn) nanocrystalline powders. *Chinese J Inorg Chem*. 2019;35(6):1101–1108.
26. Dom R, Subasri R, Radha K. Synthesis of solar active nanocrystalline ferrite, MFe_2O_4 (M: Ca, Zn, Mg) photocatalyst by electromagnetic wave irradiation. *Solid State Commun*. 2011;151(6):470–473. doi:10.1016/j.ssc.2010.12.034
27. Liu J, Qiu T, Yang J. Preparation and electromagnetic wave absorption properties of carbonyl iron particles coated with ferrite $MgFe_2O_4$. *Nonferrous Metals (Extractive Metallurgy)*. 2009;01:1–5.
28. Zhou HY, Hu L, Wan JZ. Electromagnetic wave-enhanced catalytic degradation of p-nitrophenol in soil using $MgFe_2O_4$. *Chemical Eng J*. 2016;284:54–60. doi:10.1016/j.cej.2015.08.103

29. Tian N, Wang JW, Li F. Enhanced electromagnetic wave absorption of Fe flakes with magnesium ferrite cladding. *J Magn Magn Mater*. 2012;324:4175–4178. doi:10.1016/j.jmmm.2012.07.043
30. Nishi H, Asami K, Tatsuma T. CuSnanoplates for LSPR sensing in the second biological optical window. *J Opt Mater Exp*. 2016;6 (4):1043–1049. doi:10.1364/OME.6.001043
31. Zhou DL, Liu DL, Xu W. Observation of considerable upconversion enhancement induced by $Cu_{2-x}S$ plasmon nanoparticles. *ACS Nano*. 2016;105:5169–5179. doi:10.1021/acsnano.6b00649
32. Zhang B, Shan Y, Chen K. A facile approach to fabricate of photothermal functional Fe_3O_4@CuS microspheres. *J Mater Chem Phys*. 2017;193:82–88. doi:10.1016/j.matchemphys.2017.01.079
33. Zhang M, Zhang W, Liu Y. A new class of blue-LED-excitable NIR-II luminescent nanoprobesbased on lanthanide-doped CaS nanoparticles. *Angew Chem Int Ed*. 2019;58:9556–9560. doi:10.1002/anie.201905040
34. Lechevallier S, Hammer P, Caiut MAJ. APTES-modified Re_2O_3:Eu^{3+} luminescent beads: structure and properties. *J Langmuir*. 2012;28 (8):3962–3971. doi:10.1021/la204469f
35. Zhang XL, Wang C, Ren SM. Study on quantitative analysis method of ibuprofen content in sustained-release capsules by NMR. *Chin J Marine Drugs*. 2014;01:1–9.
36. Konstan MW. Effect of ibuprofen on neutrophil migration in vivo in cystic fibrosis and healthy subjects. *J Pharmacol Exp Ther*. 2003;306 (3):1086–1091. doi:10.1124/jpet.103.052449
37. Yu Y, Song MY, Chen CL. Bortezomib-encapsulated CuS/Carbon dots nanocomposites for enhanced photothermal therapy via stabilization of polyubiquitinated substrates in the proteasomal degradation pathway. *ACS Nano*. 2020. doi:10.1021/acsnano.0c05332
38. Chen P, Cui B, Cui XR, Zhao WW, Bu YM, Wang YY. A microwave- triggered controllable drug delivery system based on hollow-mesoporous cobalt ferrite magnetic nanoparticles. *J Alloys Compd*. 2017;699:526–533.